Highly Unsaturated Hydrogenated Silicon Clusters, Si_nH_x (n = 3−10, x = 0−3), in Flash Pyrolysis of Silane and Disilane

Steven D. Chambreau, Liming Wang, and Jingsong Zhang*

Department of Chemistry, University of California, Riverside, California 92521

Received: June 27, 2001; In Final Form: November 19, 2001

Bare and partially hydrogenated neutral silicon clusters, Si_nH_x (n = 3−10, x = 0−3), were produced upon flash pyrolysis of dilute (1%) mixtures of disilane, Si_2H_6, in Ar and of silane, SiH_4, in He at temperatures above ∼1000 K. Immediately following the flash pyrolysis of the precursors (on an ∼20 μs time scale), the clusters were isolated in a supersonic molecular beam and detected by single vacuum ultraviolet (VUV) photon (λ = 118.2 or 121.6 nm) ionization time-of-flight mass spectrometry (TOFMS). The clusters produced were similar for both precursors with Si_nH_x (n = 4, 6, 7, 10) being significantly populated and Si_6H_x being the most abundant, consistent with the known "magic numbers" of Si clusters. Hydrogen contents in these Si_nH_x clusters were small with typical hydrogen mole fractions near 10%. The most stable structures of the Si_6H and Si_6H_2 clusters were identified using ab initio quantum mechanical methods. Initial thermal decomposition intermediates and reaction products, such as SiH_2, Si_2H_4, Si_2H_2, trisilanes, and tetrasilanes, were also observed by TOFMS.

Introduction

Interest in the formation of silicon clusters, including bare and hydrogenated neutrals and ions, has stemmed from their roles in Si thin film formation by chemical vapor deposition (CVD),[1−3] amorphous Si (a-Si:H) film growth,[4,5] and Si nanoparticle production.[6−10] Typical precursors for these processes include SiH_4 and Si_2H_6. While hydrogenated Si cluster formation hinders the deposition rate of crystalline Si in CVD by contaminating the surface, it is believed to enhance the growth of a-Si:H and is the initial step for the gas-phase production of Si nanoparticles.[2,3] Many experimental and theoretical studies have been carried out to investigate growth mechanisms,[2,3,11] underlying thermochemistry,[2,12] and stable geometries and energetics of neutral silicon clusters[13−20] and hydrogenated silicon clusters[21−26] and their corresponding ions.[15,25,27−31] To accurately describe homogeneous particle growth, complex kinetic and thermodynamic models have been proposed that suggest likely growth mechanisms.[2,3,11] However, particle growth processes remain somewhat unclear. Better understanding of silicon cluster formation will allow greater control over CVD rates and film contamination and provide greater selectivity of the desirable properties of Si thin films, a-Si:H, and Si nanoparticles.

Experimental production of neutral gas-phase Si clusters of up to 200 atoms has been carried out by laser ablation of pure Si with the resulting clusters being entrained in a molecular beam.[9,27] More recently, pure Si clusters have been produced by CO_2 laser-induced pyrolysis of silane followed by supersonic expansion of the resulting clusters into a molecular beam.[6] Other conventional methods of pyrolysis of silane and disilane have resulted in the production of silicon particles (>5 nm) that contain ∼10−30% mole fraction of hydrogen, have near saturation surface coverage with hydrogen, and are suspected precursors to a-Si:H growth.[2,3,11,32]

* To whom correspondence should be addressed. Fax: (909) 787-4713. E-mail: jingsong.zhang@ucr.edu. Also at: Air Pollution Research Center, University of California, Riverside, California 92521.

In this study, we describe the production, isolation, and detection of small bare and partially hydrogenated neutral silicon clusters, Si_nH_x (n = 3−10, x = 0−3), which, to our knowledge, have not previously been observed experimentally in the pyrolysis of silane and disilane. In addition, ab initio quantum mechanical calculations on Si_6H_{0-2} clusters are carried out to determine the most stable structures for these species.

Experimental and Computational Methods

The pyrolysis experiment and the experimental setup have been described previously.[33−36] Flash pyrolysis and cluster production were carried out by expanding a gas mixture of 1% silane or disilane in He or Ar at a total backing pressure of 1.3 atm through a heated SiC tube (10 mm heated length, 2 mm o.d., 1 mm i.d., Carborundum). The gas samples (silane, 99.998%, Matheson; disilane, 99.998%, Aldrich Chemicals) were used without further purification. The design for the pyrolysis source was based on that of Chen and co-workers.[33,36] The nozzle temperature was monitored with a type c thermocouple (Omega), which was calibrated to the internal temperature of the SiC tube. Fluid properties of the gas flow in the SiC tube were investigated at elevated temperatures and at 1−2 atm backing pressure (i.e., under conditions similar to our experiment).[33,36] The results indicated that the gas flow was nearly sonic in the short heated region, giving a small residence time on the order of ∼20 μs. Furthermore, the gas pressure at the exit of the tube was still sufficient to produce a supersonic expansion and cooling.[33,36]

The products and undecomposed parent molecules exited the heated tube and supersonically expanded into the vacuum chamber (at $<5 \times 10^{-4}$ Torr with the molecular beam on), where they were skimmed and passed into the photoionization region of a Wiley−McLaren type linear time-of-flight mass spectrometer (TOFMS).[37] The pyrolysis products were ionized by single vacuum ultraviolet (VUV) photon ionization at λ = 118.2 nm (10.49 eV) or 121.6 nm (10.20 eV), and the TOF

10.1021/jp012451r CCC: $22.00 © 2002 American Chemical Society
Published on Web 05/01/2002

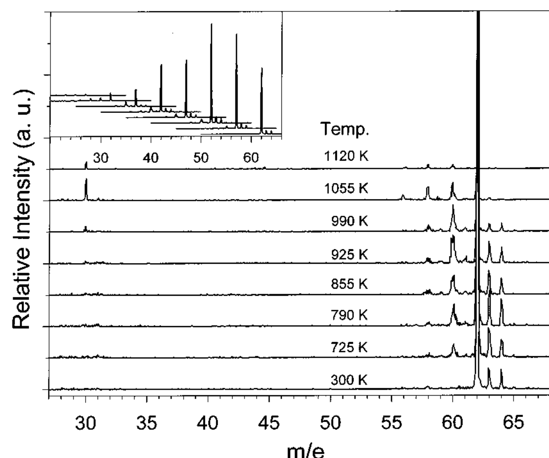

Figure 1. Mass spectra of pyrolysis of disilane (1% in He at 1.3 atm total backing pressure) between room temperature and 1120 K by using flash pyrolysis/supersonic jet/VUV photoionization TOFMS. Photoionization energy is 10.20 eV at 121.6 nm. Baselines of the TOF mass spectra are offset for clarity. The disilane peaks (*m*/*e* 62) are off scale and are shown in the inset (with both mass and baseline shifted for clarity).

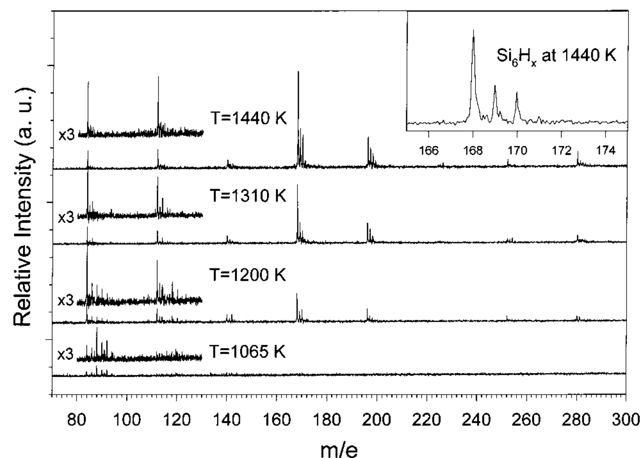

Figure 2. Si_nH_x formation upon flash pyrolysis of disilane (1% in Ar at 1.3 atm total backing pressure) between 1065 and 1440 K, detected using 10.49 eV photoionization/TOFMS. Baselines of the TOF mass spectra are offset for clarity.

mass spectra were recorded on a digital storage oscilloscope (Tektronix TDS3032, 300 MHz) or a multichannel scaler (EG&G, Turbo-MCS). The 118.2 nm radiation was produced by frequency tripling the 355 nm output from a Nd:YAG laser in a Xe cell (~50 Torr), and the 121.6 nm radiation was produced by tripling 365 nm radiation from a dye laser in a Kr cell (~80 Torr). The VUV radiation was focused by a MgF_2 lens through a small aperture into the photoionization zone, while the fundamental 355 or 365 nm UV beam diverged in this region. Without Xe or Kr, the tripling medium for VUV generation, no ion signals were observed for SiH_4 or Si_2H_6 pyrolysis at all temperatures, indicating negligible multiphoton ionization (MPI) and secondary electron-impact ionization (EI) by the fundamental UV radiation alone. MPI and fragmentation due to both VUV and UV photons (e.g., UV photodissociation of silane and polysilane parent ions after VUV photoionization) was also negligible, as indicated, for example, by little or no fragmentation in the room-temperature Si_2H_6 mass spectrum at 121.6 nm (Figure 1).

After performing several series of pyrolysis experiments, the inside of the heated section of the SiC tubing would become coated with amorphous Si (confirmed by scanning electron microscope and energy-dispersive X-ray spectroscopy), and the amount of the Si clusters observed in the gas phase also decreased. To ensure that Si deposition did not effect our results, the data presented in this paper were obtained with fresh SiC tubing and before significant Si build-up in the tube.

Ab initio calculations were performed by using the Gaussian 98 program.[38] Silicon cluster geometries were preoptimized by using Hartree–Fock (HF) or density functional theory (DFT) B3LYP methods and then refined at the second-order Møller–Plesset perturbation theory (MP2) level of theory using a polarized triple-ζ basis set, 6-311G(d,p). Vibrational frequency calculations were subsequently carried out to verify the optimized MP2 structures to be the (local) minima on the potential energy surface or the saddle points. For zero-point energy (ZPE) calculations, the MP2/6-311G(d,p) vibrational frequencies were scaled by 0.975.[39] Single-point energy calculations were carried out on the MP2/6-311G(d,p) geometries at the Gaussian-3 (G3) level of theory.[40,41] These calculations effectively obtained a QCISD(T, FU)/G3Large theory level of electron correlation, making certain assumptions on the additivity of calculations and including spin–orbital corrections and high-level corrections (HLC, correcting for nonadditivity in the calculations). The HLC used in this study are those from G3 theory with molecular geometries and zero-point energies calculated by DFT-B3LYP/6-31G(d).[41] Calculations of the clusters were restricted to singlet (for Si_6 and Si_6H_2) and doublet (for Si_6H) states.

Results and Discussion

Pyrolysis of Si_2H_6 and Formation of Si_nH_x Clusters. Initial pyrolysis products of disilane, including free-radical intermediates, were detected by VUV TOFMS. The pyrolysis products, including SiH_2, Si_2H_4, Si_2H_2, and Si_2, were identified at temperatures up to 1120 K (Figure 1). These results largely confirmed the previously proposed decomposition and dehydrogenation mechanisms of disilane:[2,3,42–47]

$$Si_2H_6 \leftrightarrow SiH_4 + SiH_2 \quad (1)$$

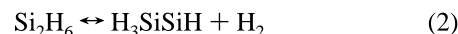
$$Si_2H_6 \leftrightarrow H_3SiSiH + H_2 \quad (2)$$

$$H_3SiSiH \leftrightarrow H_2SiSiH_2 \quad (3)$$

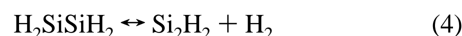
$$H_2SiSiH_2 \leftrightarrow Si_2H_2 + H_2 \quad (4)$$

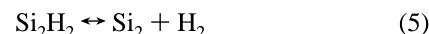
$$Si_2H_2 \leftrightarrow Si_2 + H_2 \quad (5)$$

Further details of the pyrolysis of Si_2H_6 can be found in a separate publication.[48] At moderate pyrolysis temperatures, $T < 1000$ K, no cluster formation was observed. These intermediate species (in eqs 1–5), however, play important roles in the formation of polysilanes, Si_n and Si_nH_x clusters, as discussed below.

Upon the pyrolysis of disilane at elevated temperatures, $T > 1000$ K, mass peaks corresponding to Si clusters were detected (Figure 2). At disilane pyrolysis temperatures above ~1065 K, *m*/*e* peaks at 84–92 appeared, indicating the production of Si_3H_x ($x = 0$–8) species, which range from bare and partially hydrogenated Si_3 clusters to fully saturated trisilane. Si_3 clusters with an even number of hydrogen atoms, that is, Si_3H_x ($x = 0, 2, 4, 6, 8$), seemed to be preferentially populated. With increasing temperature, a shift of the mass peak pattern from higher *m*/*e* toward *m*/*e* 84, along with a slight increase of the *m*/*e* 84 peak intensity, was observed implying subsequent dehydrogenation of the Si_3H_x species. This process is similar

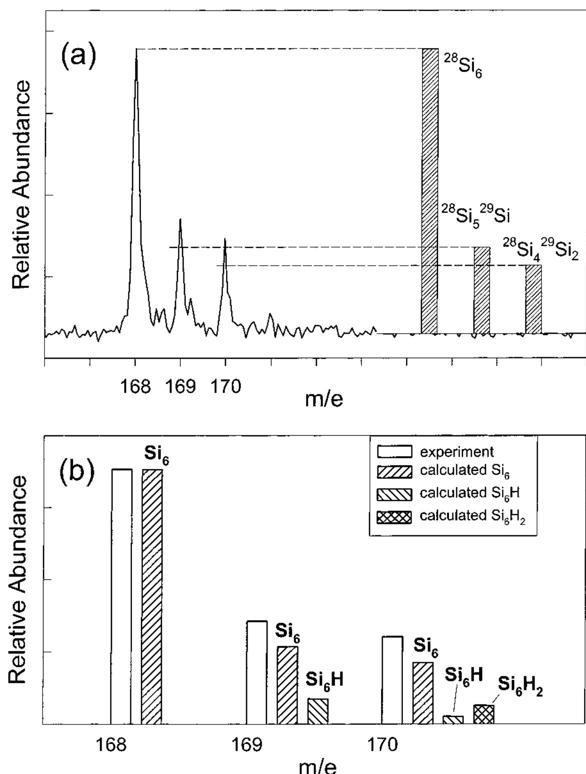

Figure 3. Modeling of contributions of hydrogenated silicon clusters: (a) experimental mass peaks of Si_6H_x from disilane pyrolysis at 1440 K versus scaled theoretical mass pattern and contribution of pure Si_6 cluster. The extra intensities in the experimental mass peaks are due to hydrogenated silicon clusters. Panel b shows the experimental mass peak intensities versus calculated contributions of Si_6, Si_6H, and Si_6H_2 clusters. This Si_6H_x spectrum is chosen for its high resolution; hydrogen contents in other Si_6H_x samples are higher. See text for more details.

to the dehydrogenation of Si_2H_6, and at the highest temperature in this study, 1440 K, most of the Si_3H_x clusters were in the bare Si_3 form. At temperatures $T \geq 1200$ K, in addition to the *m/e* 84−92 peaks for Si_3H_x, a series of new peaks appeared at *m/e* 112−120, 140−143, 168−171, 196−199, 252−255, and 280−283, which correspond to Si_nH_x ($n = 4-7, 9, 10$) clusters. Clusters larger than $Si_{10}H_x$ were not observed in this experiment. At 1200 K, *m/e* 118, 120, and 122 peaks were the hydrogen-rich tetrasilane species Si_4H_6, Si_4H_8, and Si_4H_{10}, respectively. Similar to the temperature dependence of the trisilane peaks (*m/e* 84−92), the hydrogen-rich tetrasilane species (*m/e* 118, 120, and 122) disappeared above ~1300 K and bare Si_4 clusters predominated, indicating dehydrogenation of Si_4H_x. Higher Si_nH_x clusters (with $n \geq 5$) were dominated by highly unsaturated species (with $x \leq 3$) at and above 1200 K. As the temperature was increased above 1200 K, the intensities of the Si_6H_x, Si_7H_x, and $Si_{10}H_x$ peaks increased significantly with increasing temperature, while the other cluster peaks remained at approximately the same heights. Interestingly, Si_8H_x was absent at all temperatures, and Si_5H_x and Si_9H_x were of small intensities, while Si_6H_x and Si_7H_x were the most abundant species at elevated temperatures. Note that because photoionization cross sections of the various Si_nH_x clusters at 118.2 nm are not known, any possible corrections for photoionization efficiencies cannot be made.

Experimental intensities of each mass peak in the TOF mass spectra were obtained using Gaussian peak fitting. To determine the extent of hydrogenation within each cluster, contributions from bare Si_n clusters were modeled using Si isotopic abundances that were then subtracted from the experimental mass peak intensities. On the basis of the isotope natural abundances of ^{28}Si, ^{29}Si, and ^{30}Si (92.2%, 4.7%, and 3.1%, respectively), mass peak patterns of the Si_n clusters, that is, relative peak areas of mass $^{28}Si_n$, $^{28}Si_n + 1$ ($^{28}Si_{n-1}{}^{29}Si$), $^{28}Si_n + 2$ ($^{28}Si_{n-2}{}^{29}Si_2$ and $^{28}Si_{n-1}{}^{30}Si$), etc., were calculated. As the lowest mass for each group of Si_nH_x cluster corresponds to the isotopically pure $^{28}Si_n$, the calculated isotopic mass peak pattern of Si_n can be scaled to the experimental mass peak intensities of Si_n at the $^{28}Si_n$ mass peak. At the experimental mass peak $^{28}Si_n + 1$, the only contributors are $^{28}Si_{n-1}{}^{29}Si$ and $^{28}Si_nH$, and thus by subtracting the calculated and scaled contribution of $^{28}Si_{n-1}{}^{29}Si$ from the experimental mass $^{28}Si_n + 1$ peak, the relative amount of $^{28}Si_nH$ was determined. Now knowing the contribution from $^{28}Si_nH$, the isotopic contributions to the experimental mass $^{28}Si_n + 2$ peak from $^{28}Si_{n-1}{}^{29}SiH$ (calculated and scaled from the isotopic mass pattern of Si_nH), as well as from $^{28}Si_{n-2}{}^{29}Si_2$ and $^{28}Si_{n-1}{}^{30}Si$ (from the mass pattern of Si_n), were subtracted from the experimental mass $^{28}Si_n + 2$ peak, yielding the relative amount of $^{28}Si_nH_2$. Successive iterations of this process allowed for the determination of relative amounts of clusters having higher hydrogen content. An example of this modeling for the Si_6H_x clusters is shown in Figure 3. In general, Si_nH_x clusters with n values up to 7 and x values up to 10 were considered in the modeling, but for $n \geq 5$, only clusters with $x < 3$ were observed at all temperatures. Results for the modeling of Si_nH_x clusters from disilane pyrolysis are shown in Table 1, in which the relative populations of the Si_nH_x clusters, as well as the normalized ratios to their corresponding bare Si_n clusters, are reported. With sufficient dehydrogenation above 1300 K, the amount of Si_nH ranges from ~0 to ~40% of the bare cluster population, Si_nH_2 is 0 to ~30%, and Si_nH_3 from 0 to ~5%.

TABLE 1: Relative Population of the Bare and Hydrogenated Si_nH_x Clusters Formed upon Pyrolysis of Disilane at Elevated Temperatures[a]

species	1065 K	1200 K	1310 K	1440 K
Si_3	4 (1.0)	15 (1.0)	12 (1.0)	14 (1.0)
Si_3H	0 (0.0)	0 (0.0)	2 (0.2)	2 (0.1)
Si_3H_2	3 (0.8)	5 (0.3)	3 (0.2)	1 (0.1)
Si_3H_3	2 (0.5)	0 (0.0)		
Si_3H_4	8 (2.0)	5 (0.3)		
Si_3H_6	5 (1.2)	4 (0.3)		
Si_3H_7	3 (0.7)	0 (0.0)		
Si_3H_8	5 (1.3)	3 (0.2)		
Si_4		10 (1.0)	10 (1.0)	14 (1.0)
Si_4H		5 (0.5)	1 (0.1)	0.3 (0.0)
Si_4H_2		4 (0.4)	3 (0.3)	
Si_4H_3		0 (0.0)		
Si_4H_6		5 (0.5)		
Si_4H_8		4 (0.4)		
Si_5		6 (1.0)	6 (1.0)	7 (1.0)
Si_5H		1 (0.2)	2 (0.3)	2 (0.3)
Si_5H_2		4 (0.7)	1 (0.1)	2 (0.3)
Si_5H_3		1 (0.1)		
Si_6		21 (1.0)	43 (1.0)	70 (1.0)
Si_6H		2 (0.1)	2 (0.0)	7 (0.1)
Si_6H_2		4 (0.2)		5 (0.1)
Si_6H_3				
Si_7		10 (1.0)	15 (1.0)	23 (1.0)
Si_7H		1 (0.1)	6 (0.4)	3 (0.3)
Si_7H_2		0.0 (0.0)		1 (0.0)
Si_7H_3				1 (0.0)

[a] Values reported in parentheses are normalized to the corresponding bare cluster population. Error is ±10% of the listed value.

The growth of polysilanes, Si_nH_{2n+2}, likely arises from the successive insertion of silylene SiH_2 into the lower silanes,[2,42−48] such as,

$$SiH_2 + Si_2H_6 \leftrightarrow Si_3H_8 \quad (6)$$

$$SiH_2 + Si_nH_{2(n+1)} \leftrightarrow Si_{n+1}H_{2(n+2)} \quad (7)$$

The formation of SiH_2, starting at a pyrolysis temperature slightly below that for the formation of polysilanes and silicon clusters, is one indication that SiH_2 plays a role in their formations, and this mechanism has been largely accepted.[2,42−47] At elevated temperatures ($T \geq 1300$ K), the bare Si_n clusters become predominant in the mass spectra, with partially hydrogenated species present to a lesser extent. The extent of hydrogenation, or lack thereof, could be due to H_2 or SiH_4 elimination from thermally activated polysilanes or chemically activated polysilanes (which are produced by SiH_2 insertion but are not yet stabilized) or both:

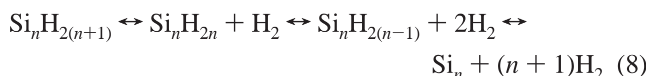

$$Si_nH_{2(n+1)} \leftrightarrow Si_nH_{2n} + H_2 \leftrightarrow Si_nH_{2(n-1)} + 2H_2 \leftrightarrow Si_n + (n+1)H_2 \quad (8)$$

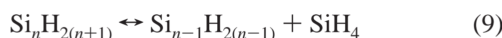

$$Si_nH_{2(n+1)} \leftrightarrow Si_{n-1}H_{2(n-1)} + SiH_4 \quad (9)$$

At elevated temperatures, these dehydrogenation processes could compete efficiently with the dissociation to SiH_2 (reverse of reaction 7), and thus, bare silicon clusters and highly unsaturated hydrogenated silicon clusters dominate, consistent with the absence of polysilane species for $n \geq 5$. Alternatively, larger bare and highly unsaturated Si_nH_x ($n \geq 6$) clusters could be formed by condensation of smaller bare and highly unsaturated silicon clusters, for example, $Si_m + Si_{n-m} \leftrightarrow Si_n$ and $Si_mH_y + Si_{n-m}H_{x-y} \leftrightarrow Si_nH_{x-2} + H_2$, either within the pyrolysis region or during the supersonic expansion. The pathway of forming Si_nH_x with an odd number of H atoms, such as Si_nH, might involve elimination of a H atom from the dihydrogenated clusters.

The predominance of the Si_6H_x clusters (also observed in silane pyrolysis discussed below) could imply a thermodynamic stability of the Si_6 cluster relative to the others, although kinetic factors may also be important. The Si_8H_x clusters were not observed in any significant amount, presumably because of a lack of stability or slow kinetics of its production. Indeed, at high temperatures at which bare silicon clusters dominate, the cluster distributions in the pyrolysis of Si_2H_6 (as well as of SiH_4, shown later) indicate significant populations of Si_nH_x ($n = 4$, 6, 7, 10) clusters, consistent with the "magic numbers" identified in previous studies.[16,17,27] It is conceivable that these small bare and highly unsaturated silicon clusters, which are produced at the early stage of pyrolysis, could serve as the "seeds" and facilitate homogeneous gas-phase nucleation of large silicon particles in CVD of silicon from Si_2H_6 and SiH_4.[2,11] Interestingly, the small hydrogen content of the Si_nH_x clusters (Tables 1 and 2), after extensive dehydrogenation from the H/Si ratio of ~2:1 in polysilanes, is slightly less than or comparable to that in the large silicon particles generated by conventional gas-phase pyrolysis of silane and disilane.[2,3,11,32]

Pyrolysis of SiH_4 and Formation of Si_nH_x Clusters. In the pyrolysis of silane, the generation of SiH_2 was also directly identified by VUV TOFMS:[48]

$$SiH_4 \leftrightarrow SiH_2 + H_2 \quad (10)$$

In addition, the production of Si_2H_6 (reverse of reaction 1), along with the subsequent decomposition and reactions of Si_2H_6 (reactions 2−6) were also observed,[48] in agreement with the previously proposed mechanisms.[45−47] As in the high-temperature pyrolysis of disilane, Si_nH_x clusters were formed upon pyrolysis of silane beginning at a pyrolysis temperature of 1080 K, as shown in Figure 4. The intensity pattern and temperature dependence of these cluster peaks followed a similar trend to those when Si_2H_6 is the precursor, although the peaks appeared with lower intensity and had lower mass resolution. Although less well-resolved compared to those in disilane pyrolysis in Ar, the approximate extent of hydrogenation within each of these clusters formed upon pyrolysis of silane in He can still be extracted by modeling. The difference in resolution might be due to the greater cooling effect of Ar (for disilane) versus He (for silane) upon supersonic expansion. Similar to the disilane experiment, the mass peaks appeared at 84−88, 112−116, 140−144, 168−172, 196−200, 252−255, and 280−283 at and above 1080 K, corresponding to the Si_nH_x ($n = 3$−7, 9, 10) clusters. From pyrolysis temperatures 1220−1530 K, the Si_6H_x and Si_7H_x cluster peaks increased most significantly, while other cluster peaks grew to a lesser extent, similar to the temperature dependence of the mass peaks in disilane pyrolysis. Also, the

TABLE 2: Relative Population of the Bare and Hydrogenated Si_nH_x Clusters in Silane Pyrolysis at Elevated Temperatures[a]

species	1080 K	1220 K	1365 K	1530 K
Si_3	2 (1.0)	2 (1.0)	4 (1.0)	3 (1.0)
Si_3H	0.4 (0.2)	2 (1.0)	1 (0.3)	2 (0.8)
Si_3H_2	1 (0.5)	0.5 (0.3)		
Si_4	2 (1.0)	3 (1.0)	7 (1.0)	6 (1.0)
Si_4H	0.7 (0.4)	2 (0.6)	3 (0.5)	6 (1.1)
Si_4H_2	2 (1.0)	0.6 (0.2)	0.4 (0.1)	2 (0.3)
Si_4H_3	0.6 (0.3)	0 (0.0)	0.6 (0.1)	
Si_4H_4	1 (0.5)	0.6 (0.2)	0.8 (0.1)	
Si_5	1 (1.0)	4 (1.0)	6 (1.0)	8 (1.0)
Si_5H	0.8 (0.8)	2 (0.5)	3 (0.4)	6 (0.8)
Si_5H_2		0.8 (0.2)	3 (0.5)	2 (0.2)
Si_5H_3		0.6 (0.2)	1 (0.2)	2 (0.2)
Si_6	2 (1.0)	21 (1.0)	40 (1.0)	58 (1.0)
Si_6H	1 (0.5)	10 (0.5)	20 (0.5)	35 (0.6)
Si_6H_2	0.3 (0.1)	1 (0.0)	10 (0.2)	9 (0.1)
Si_6H_3	0.6 (0.3)	1 (0.0)	5 (0.1)	5 (0.1)
Si_7	2 (1.0)	18 (1.0)	27 (1.0)	16 (1.0)
Si_7H	1.5 (0.7)	9 (0.5)	15 (0.5)	12 (0.8)
Si_7H_2	0.5 (0.2)	2 (0.1)	4 (0.1)	10 (0.6)
Si_7H_3	0.3 (0.1)	2 (0.1)	5 (0.2)	5 (0.3)

[a] Values reported in parentheses are normalized to the corresponding bare cluster population. Error is ±10% of the listed value.

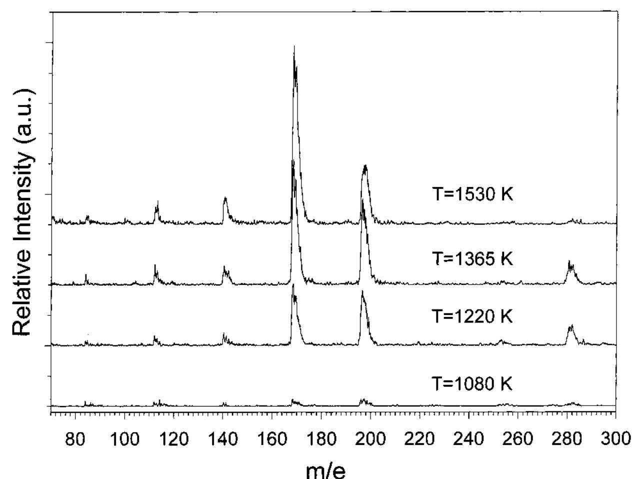

Figure 4. Si_nH_x formation upon flash pyrolysis of silane (1% in He) between 1080 and 1530 K, detected using 10.49 eV photoionization/TOFMS. The mass spectra are shifted for clarity. The lower mass resolution compared to that in Figure 2 might be due to the less efficient cooling of the He carrier gas in the molecular beam.

Si_6H_x clusters remained predominant, along with a large population of Si_7H_x. This remarkable similarity in the mass pattern and temperature dependence of the Si clusters in both SiH_4 and Si_2H_6 pyrolysis suggests essentially the same cluster growth mechanisms.

Similar to the treatment for disilane pyrolysis, the partially resolved experimental TOF mass spectra are fitted using Gaussian peaks to model the experimental mass peak intensities. Subsequently, the amount of bare silicon and hydrogenated silicon clusters are modeled based on Si isotope abundance. Results for the silane cluster modeling are listed in Table 2. At $T \geq 1220$ K, the Si_nH content ranges from ~20% to ~110% of the bare Si cluster population, while Si_nH_2 and Si_nH_3 range from 0 to ~60% and 0 to ~30%, respectively. Compared to the disilane pyrolysis, there is a greater extent of hydrogenation involved in the Si_nH_x formation with SiH_4 as a precursor. Although the mechanisms for cluster growth are similar, an initial step to convert SiH_4 to Si_2H_6 (reverse reaction 1) is required in SiH_4 pyrolysis, which could slow the growth of polysilanes and their dehydrogenation. In addition, the increased hydrogenation in the clusters with silane vs disilane might be due to the higher H/Si ratio in silane (4:1 vs 3:1 in disilane). For example, a larger concentration of the H_2 product could increase the extent of H_2 addition to clusters, that is, the reverse reactions of dehydrogenation (e.g., reverse reactions 2 and 10) in the chemical equilibrium.[2]

Structure and Stability of Si_6H_x ($x = 0-2$) Clusters by ab Initio Calculations. Because there is no previous experimental observation for the hydrogenated Si clusters and no structural information available from the TOF mass spectra in this study, we investigate structures and energetics of the observed Si_nH_x clusters using ab initio quantum-mechanical calculations.[49] The results for Si_6H_x ($x = 0-2$) are reported here.

Because the bare Si_6 has been extensively characterized,[13-20] it serves to establish the computational method for the hydrogenated Si clusters in this study. The MP2 method has proven to be the proper method for the Si_n clusters because it successfully predicted the experimental vibrational frequencies of Si_4, Si_6, and Si_7 from IR and Raman spectroscopy.[13,14] The MP2/6-31G(d) calculations predicted a lowest-energy Si_6 cluster with D_{4h} symmetry (consistent with IR and Raman spectroscopy), while the most stable Si_6 structures by HF (with 6-31G(d) basis set) and DFT methods were distorted from the D_{4h} symmetry and reduced to C_{2v} and C_s, respectively.[16-18,22] Our MP2/6-311G(d,p) optimization reproduces the same stable D_{4h} structure of Si_6 (Figure 5 and Table 3),[13,15] and the calculated vibrational frequencies of Si_6 are in good agreement with the experimental values (Table 3).[13-15] Judged by the location and bonding, two types of Si atoms are identified in the D_{4h} Si_6 cluster: (i) two atoms on the C_4 axis (atoms 1 and 2, Si_6, Figure 5) having saturated bonding with four Si-Si single bonds (to atoms 3-6) and (ii) four atoms (atoms 3-6) on the D_{4h} square plane, which are bonding deficient or less-saturated with only two Si-Si single bonds (to atoms 1 and 2). Note that a typical Si-Si single bond (such as that in polysilanes) has a bond length of <2.5 Å. On the basis of the results for Si_6, the MP2/6-311G(d,p) method is chosen for the studies of Si_6H and Si_6H_2. The most stable structures of Si_6H_x ($x = 0-2$) obtained in this work are shown in Figure 5, and their geometric parameters, vibrational frequencies, and energetics are listed in Tables 3 and 4.

The Si_6H cluster could have both the traditional H-Si single bonds and the nonclassical H-bridged Si-Si bonds and H-bridged Si-Si-Si triangular surfaces. The H-bridged Si-Si

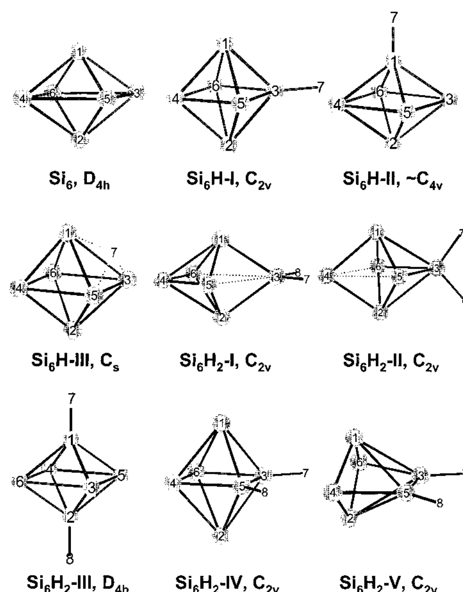

Figure 5. Stable structures of the Si_6H_{0-2} clusters optimized at MP2/6-311G(d,p) level of theory. Geometric parameters, vibrational frequencies, and energetics are listed in Tables 3 and 4.

bonds have been long recognized in hydrogen-deficient small silicon species such as Si_2H_2.[50] Our geometry optimization and vibrational frequency calculations indicate that the H-Si single bonds and the H-bridged Si_3 triangular surface are (local) minima on the potential energy surface, while the H-bridged Si-Si edges are saddle points.

H-atom bonding to a saturated Si atom on the cap results in an approximate C_{4v} structure (Si_6H-II, Figure 5 and Table 3). MP2/6-311G(d,p) failed in geometry optimization starting with C_{4v}, but it reached the nearly C_{4v} geometry when started from a C_s symmetry as obtained in DFT-BPW91/DNP.[16,29] Vibrational frequencies also indicate a near degeneracy, in which an E-mode in C_{4v} is reduced to A′ + A″ in C_s. The Si_6 frame of Si_6H-II is only slightly distorted from Si_6, with a maximum Si-Si distance change of 0.05 Å, and the vibrational modes of the bare Si_6 are essentially retained in Si_6H-II with clear symmetry correlations. The H-Si bond energy in Si_6H-II is 148 kJ/mol, much less than that of H-Si in SiH_4 (ranging from 287 to 371 kJ/mol).[51] H-atom bonding to a less-saturated Si atom in the square plane results in a C_{2v} Si_6H-I structure that is significantly distorted from the bare Si_6 (Table 3 and Figure 5). The distance between Si-3 (the binding site) and Si-5/6 is shortened from 2.746 Å in the bare Si_6 to 2.451 Å, and that between Si-3 and Si-1/2 from 2.364 to 2.313 Å; the H bonding in Si_6H-I seems to strengthen the adjacent Si-Si bonds. Si_6H-I is the most stable Si_6H, with a H-Si bond energy of 204 kJ/mol (Table 4) and thus is likely the one observed in the TOF mass spectra of this study. The structure with a H-bridged Si_3 triangular surface bond (Si_6H-III, Figure 5), which was previously predicted by non-orthogonal tight-binding molecular dynamics,[20] has a bond energy of only 74 kJ/mol at G3 level of theory, much smaller than those of the H-Si single bonds. The preference of the single, rather than the H-bridged, H-Si bonds in Si_6H is consistent with the trend toward the single H-Si bonding on a bulk silicon surface that starts from Si_4H.[26]

Possible structures of Si_6H_2 with two H-atom attachments are combinations of the single H-atom ones. However, the H-bridged Si_3 surface structures are ruled out because of their high energies, and only five stationary geometries with H-Si single bonds are located (Figure 5). Si_6H_2-I and Si_6H_2-II (both C_{2v}) can be viewed as two H-Si bonds on the same less-

TABLE 3: Geometries and Vibrational Frequencies of $Si_6H_{0,1,2}$ Clusters at MP2/6-311G(d,p) Level of Theory[a]

clusters	symmetry	bond distance (Å)	vibrational frequencies (cm^{-1})
Si_6	D_{4h}	$R(1-3) = 2.364$ (2.356);[b] $R(3-5) = 2.746$ (2.734)[b]	69 (E_u, 86.0 and 87.0),[c] 175 (B_{2u}), 223 (B_{2g}, 252),[d] 303 (A_{1g}, 300),[d] 321(A_{2u}), 365 (B_{1g}, 386),[d] 410 (E_g, 404),[d] 445 (E_u, 461, 463, 458),[e] 452 (A_{1g}, 458)[d]
Si_6H-I	C_{2v}	$R(1-3) = 2.313$; $R(1-4) = 2.379$; $R(1-5) = 2.512$; $R(3-5) = 2.451$; $R(4-5) = 2.568$; $R(Si-H) = 1.482$	113 (B_2), 138 (A_1), 170 (B_1), 288 (B_1), 306 (B_2), 308 (A_2), 343 (A_1), 370 (B_2), 382 (A_1), 384 (B_1), 435 (B_1), 452 (A_1), 564 (B_2), 604 (B_1), 2143 (A_1)
Si_6H-II	C_s ($\sim C_{4v}$)	$R(1-3) = 2.361$; $R(2-3) = 2.382$; $R(3-5) = 2.7251$; $R(4-5) = 2.7247$; $R(Si-H) = 1.484$	66 (A′), 66 (A″), 187 (A′), 217 (A″), 300 (A′), 360 (A′), 363 (A′), 374 (A′), 375 (A″), 421 (A′), 421 (A″), 444 (A′), 528 (A′), 528 (A″), 2121 (A′)
Si_6H-III	C_s	$R(1-3) = 2.624$; $R(1-4) = 2.377$; $R(2-3) = 2.405$; $R(2-4) = 2.399$; $R(3-5) = 2.732$; $R(4-6) = 2.742$; $R(4-5) = 2.574$; $R(Si_3-H) = 1.788$; $R(Si_1-H) = 1.692$	122 (A′), 156 (A″), 169 (A″), 266 (A′), 286 (A′), 315 (A′), 328 (A″), 361 (A″), 363 (A′), 383 (A′), 394 (A″), 421 (A′), 907 (A″), 972 (A′), 1227 (A′)
Si_6H_2-I	C_{2v}	$R(1-3) = 2.323$; $R(1-4) = 2.385$; $R(1-5) = 2.467$; $R(4-5) = 2.348$; $R(3-5) = 3.250$; $R(Si-H) = 1.477$	52 (B_2), 154 (B_1), 189 (A_1), 391 (B_1), 299 (B_2), 320 (A_2), 330 (A_1), 344 (A_1), 412 (B_1), 433 (A_2), 441 (A_1), 453 (B_2), 473 (A_1), 555 (B_2), 665 (B_1), 979 (A_1), 2178 (A_1), 2187 (B_2)
Si_6H_2-II	C_{2v}	$R(1-3) = 2.477$; $R(1-4) = 2.288$; $R(1-5) = 2.398$; $R(4-5) = 2.907$; $R(3-5) = 2.557$; $R(Si-H) = 1.488$	27 (B_1), 133 (B_2), 171 (A_1), 253 (B_1), 271 (A_2), 293 (B_2), 314 (A_1), 351 (A_1), 387 (A_2), 405 (B_1), 410 (B_2), 416 (A_1), 478 (A_1), 551 (B_1), 588 (B_2), 1042 (A_1), 2104 (B_2), 2118 (A_1)
Si_6H_2-III	D_{4h}	$R(1-3) = 2.366$; $R(3-5) = 2.710$; $R(Si-H) = 1.474$	74 (E_u), 209 (B_{2u}), 222 (B_{2g}), 310 (A_{1g}), 361 (B_{1g}), 383 (A_{2u}), 391 (E_g), 417 (E_u), 454 (A_{1g}), 489 (E_g), 649 (E_u), 2195 (A_{1g}), 2196 (A_{2u})
Si_6H_2-IV	C_{2v}	$R(1-3) = 2.472$; $R(1-4) = 2.581$; $R(3-5) = 2.304$; $R(4-6) = 2.444$; $R(4-5) = 2.368$; $R(Si-H) = 1.495$	112 (A_2), 132 (A_1), 137 (B_2), 280 (B_2), 296 (B_1), 312 (A_2), 343 (A_1), 352 (A_1), 362 (B_1), 378 (B_2), 418 (A_1), 458 (A_1), 529 (A_2), 566 (B_2), 571 (B_1), 607 (A_1), 2134 (B_2), 2139 (A_1)
Si_6H_2-V	C_{2v}	$R(1-3) = 2.605$; $R(1-4) = 2.370$; $R(3-5) = 2.232$; $R(4-5) = 2.321$; $R(Si-H) = 1.482$	81 (A_2), 132 (B_1), 186 (A_1), 208 (B_2), 255 (B_1), 298 (A_1), 320 (A_2), 355 (A_1), 395 (B_2), 431 (B_1), 438 (A_1), 444 (B_2), 455 (A_2), 499 (A_1), 612 (B_2), 618 (A_1), 2134 (B_2), 2139 (A_1)

[a] The vibrational frequencies are scaled by 0.95.[39] Experimental or other theoretical values are in parentheses. [b] Reference 15. [c] Reference 52. [d] Reference 13. [e] Reference 14.

TABLE 4: Relative Energies (corrected for ZPE) of Si_6H_n ($n = 0-2$) Clusters with Respect to $Si_6 + n$H at Gaussian-3 Level of Theory and ZPE at MP2/6-311G(d,p) (with vibrational frequencies scaled by 0.975)[a]

clusters	symmetry	ZPE	relative energy
Si_6 (D_{4h}) + H	D_{4h}	22.6	0
Si_6H-I	C_{2v}	43.0	−204
Si_6H-II	$\sim C_{4v}$	41.5	−148
Si_6H-III	C_s	41.0	−74
Si_6 + 2H	D_{4h}	22.6	0
$Si_6 + H_2$		48.9	−432
Si_6H_2-I	C_{2v}	66.0	−483
Si_6H_2-II	C_{2v}	63.3	−413
Si_6H_2-III	D_{4h}	63.6	−488
Si_6H_2-IV	C_{2v}	62.1	−492
Si_6H_2-V	C_{2v}	61.4	−446

[a] All values are in kJ/mol.

saturated Si-atom (atom 3), Si_6H_2-III as two H−Si bonds on the two saturated Si-atoms (trans conformation in D_{4h}), Si_6H_2-IV as two H−Si bonds to two less-saturated Si-atoms (cis conformation in C_{2v}), and Si_6H_2-V as a further distortion from Si_6H_2-IV. Distortion of the Si_6 frame from the bare Si_6 is small in Si_6H_2-III, while it is large in all others. Correlation of vibrational modes between bare Si_6 and Si_6H_2-III can be easily identified as well. The lowest-energy structures are Si_6H_2-I, -III, and -IV, which have virtually the same energy. The most stable structure Si_6H_2-IV is derived from the most stable Si_6H-I, while Si_6H_2-III is from the higher energy Si_6H-II. In the two previous theoretical studies of Si_6H_2, stable structures similar to Si_6H_2-III (by DFT method)[22] and Si_6H_2-I (by MINDO/3)[24] were located. Note that structure Si_6H_2-II is unstable with respect to H_2 elimination (Table 4) and structure Si_6H_2-V is also unlikely to be observed in this experiment because of its higher energy.

The average H−Si bond energy in all of the Si_6H_2 structures is more than the largest H−Si bond energy in Si_6H. From Si_6 to Si_6H-II to Si_6H_2-III, the sequential H−Si bond energies are 148 and 340 kJ/mol, and from Si_6 to Si_6H-I to Si_6-IV, these values are 204 and 288 kJ/mol, respectively. In both cases, the second H−Si bond is as strong as that of SiH_4. This bond strength might give rise to the relatively large abundance of Si_6H_2 clusters in the experiment. On the other hand, the H_2 elimination energy for $Si_6H_2 \rightarrow Si_6 + H_2$ is less than 60 kJ/mol

for the most stable Si_6H_2 series (I, III, and IV). This is consistent with an H_2 elimination energy of 100 kJ/mol for Si_4H_2 and the general trend of decreasing elimination energy with increasing degree of unsaturation and number of multiple Si−Si bonds.[12,25] Thus, dehydrogenation of Si_6H_2 can be efficient at elevated temperatures. Among the most stable Si_6H_2 clusters, this dehydrogenation could readily occur in Si_6H_2-I (via 1,1 H_2 elimination) and Si_6H_2-IV (via 1,2 H_2 elimination), while for Si_6H_2-III, H-migration is required.

Conclusion

The first experimental evidence of production of highly unsaturated neutral Si clusters, Si_nH_x ($n = 3-10$, $x = 0-3$), in the pyrolysis of SiH_4 and Si_2H_6 is reported. Through the use of the flash pyrolysis technique, coupled with single-photon VUV TOFMS, the reactive intermediates (SiH_2, Si_2H_4, etc.), polysilane products (trisilanes and tetrasilanes), and Si_nH_x clusters are isolated and detected upon homogeneous decomposition of silane and disilane precursors. The Si_nH_x (n = 4, 6, 7, 10) clusters are significantly populated in both cases with Si_6H_x being the most abundant, in agreement with the known "magic numbers" of silicon clusters. The Si_nH_x clusters from SiH_4 pyrolysis have a higher extent of hydrogenation than do those from Si_2H_6, possibly because of the slower growth of polysilanes and the increased amount of H_2 present in the pyrolysis of silane. Production of the Si_nH_x clusters likely plays a role in homogeneous nucleation of silicon particles in industrially important processes such as CVD, a-Si:H film production, and Si nanoparticle formation. Further work is necessary to determine mechanistic pathways involved in the cluster production. The lowest-energy structures of the Si_6H_x ($x = 0-2$) clusters, as well as their geometric parameters, vibrational frequencies, and energetics, are obtained by using MP2/6-311G(d,p) quantum-mechanical calculations. The most stable structure of Si_6H is Si_6H-I, and those of Si_6H_2 are Si_6H_2-I, -III, or -IV (Figure 5), and they are likely the ones observed experimentally in our TOF mass spectra. These most stable structures of Si_6H and Si_6H_2 prefer the H−Si single bonds rather than the nonclassical H-bridged Si−Si bonds or H-bridged Si−Si−Si bonds.

Acknowledgment. This work is supported by National Science Foundation (Grants CHE-9811400 and CHE-0111635), a UC Regents' Faculty Fellowships and Faculty Development Award, and a Camille and Henry Dreyfus New Faculty Award. We acknowledge the computational support from San Diego Supercomputer Center. We thank Prof. Tom Morton for help with the calculations.

References and Notes

(1) Jasinski, J. M.; Gates, S. M. *Acc. Chem. Res.* **1991**, *24*, 9.
(2) Swihart, M. T.; Girshick, S. L. *J. Phys. Chem. B* **1999**, *103*, 64.
(3) Onischuk, A. A.; Strunin, V. P.; Ushakova, M. A.; Panfilov, V. N. *J. Aerosol Sci.* **1997**, *28*, 207.
(4) Kessels, W. M. M.; Leewis, C. M.; van de Sanden, M. C. M.; Schram, D. C. *J. Appl. Phys.* **1999**, *86*, 4029.
(5) Ruther, R.; Livingstone, J. *Infrared Phys. Technol*. **1996**, *37*, 533.
(6) Ehbrecht, M.; Huisken, F. *Phys. Rev. B: Condens. Matter Mater. Phys.* **1999**, *59*, 2975.
(7) Huisken, F.; Kohn, B.; Paillard, V. *Appl. Phys. Lett.* **1999**, *74*, 3776.
(8) Laguna, M. A.; Paillard, V.; Kohn, B.; Ehbrecht, M.; Huisken, F.; Ledoux, G.; Papoular, R.; Hofmeister, H. *J. Lumin.* **1998**, *80*, 223.
(9) Melinon, P.; Keghelian, P.; Prevel, B.; Perez, A.; Guiraud, G.; LeBrusq, J.; Lerme, J.; Pellarin, M.; Broyer, M. *J. Chem. Phys.* **1997**, *107*, 10278.
(10) Watanabe, M. O.; Miyazaki, T.; Kanayama, T. *Phys. Rev. Lett.* **1998**, *81*, 5362.
(11) Frenklach, M.; Ting, L.; Wang, H.; Rabinowitz, M. J. *Isr. J. Chem.* **1996**, *36*, 293.
(12) Katzer, G.; Ernst, M. C.; Sax, A. F.; Kalcher, J. *J. Phys. Chem. A* **1997**, *101*, 3942.
(13) Honea, E. C.; Ogura, A.; Murray, C. A.; Raghavachari, K.; Sprenger, W. O.; Jarrold, M. F.; Brown, W. L. *Nature* **1993**, *366*, 42.
(14) Li, S.; Vanzee, R. J.; Weltner, W.; Raghavachari, K. *Chem. Phys. Lett.* **1995**, *243*, 275.
(15) Xu, C. S.; Taylor, T. R.; Burton, G. R.; Neumark, D. M. *J. Chem. Phys.* **1998**, *108*, 1395.
(16) Raghavachari, K. *J. Chem. Phys.* **1986**, *84*, 5672.
(17) Raghavachari, K.; Rohlfing, C. M. *J. Chem. Phys.* **1988**, *89*, 2219.
(18) Hartke, B. *Theor. Chem. Acc.* **1998**, *99*, 241.
(19) Liu, B.; Lu, Z. Y.; Pan, B. C.; Wang, C. Z.; Ho, K. M.; Shvartsburg, A. A.; Jarrold, M. F. *J. Chem. Phys.* **1998**, *109*, 9401.
(20) Gupte, G. R.; Prasad, R. *Int. J. Mod. Phys. B* **1998**, *12*, 1737.
(21) Swihart, M. T.; Girshick, S. L. *Chem. Phys. Lett.* **1999**, *307*, 527.
(22) Miyazaki, T.; Uda, T.; Stich, I.; Terakura, K. *Chem. Phys. Lett.* **1996**, *261*, 346.
(23) Kalcher, J.; Sax, A. F. *Chem. Phys. Lett.* **1996**, *259*, 165.
(24) Meleshko, V.; Morokov, Y.; Schweigert, V. *Chem. Phys. Lett.* **1999**, *300*, 118.
(25) Wang, W. N.; Tang, H. R.; Fan, K. N.; Iwata, S. *J. Chem. Phys.* **2001**, *114*, 1278.
(26) Xu, C. S.; Taylor, T. R.; Burton, G. R.; Neumark, D. M. *J. Chem. Phys.* **1998**, *108*, 7645.
(27) Fuke, K.; Tsukamoto, K.; Misaizu, F.; Sanekata, M. *J. Chem. Phys.* **1993**, *99*, 7807.
(28) Jasinski, J. M. *J. Vac. Sci. Technol., A* **1995**, *13*, 1935.
(29) Miyazaki, T.; Uda, T.; Stich, I.; Terakura, K. *Chem. Phys. Lett.* **1998**, *284*, 12.
(30) Watanabe, M. O.; Murakami, H.; Miyazaki, T.; Kanayama, T. *Appl. Phys. Lett.* **1997**, *71*, 1207.
(31) Kessels, W. M. M.; Leewis, C. M.; Leroux, A.; van de Sanden, M. C. M.; Schram, D. C. *J. Vac. Sci. Technol., A* **1999**, *17*, 1531.
(32) Onischuik, A. A.; Strunin, V. P.; Samoilova, R. I.; Nosov, A. V.; Ushakova, M. A.; Panfilov, V. N. *J. Aerosol Sci.* **1999**, *28*, 1425.
(33) Kohn, D. W.; Clauberg, H.; Chen, P. *Rev. Sci. Instrum.* **1992**, *63*, 4003.
(34) Boyle, J.; Pfefferle, L.; Lobue, J.; Colson, S. *Combust. Sci. Technol.* **1990**, *70*, 187.
(35) Chambreau, S. D.; Zhang, J. S.; Traeger, J. C.; Morton, T. H. *Int. J. Mass Spectrom*. **2000**, *199*, 17.
(36) Friderichsen, A. V.; Radziszewski, J. G.; Nimlos, M. R.; Winter, P. R.; Dayton, D. C.; David, D. E.; Ellison, G. B. *J. Am. Chem. Soc.* **2001**, *123*, 1977.
(37) Lubman, D. M.; Jordan, R. M. *Rev. Sci. Instrum.* **1985**, *56*, 373.
(38) Frisch, M. J.; Trucks, G. W.; Schlegel, H. B.; Scuseria, G. E.; Robb, M. A.; Cheeseman, J. R.; Zakrzewski, V. G.; Montgomery, J. A., Jr.; Stratmann, R. E.; Burant, J. C.; Dapprich, S.; Millam, J. M.; Daniels, A. D.; Kudin, K. N.; Strain, M. C.; Farkas, O.; Tomasi, J.; Barone, V.; Cossi, M.; Cammi, R.; Mennucci, B.; Pomelli, C.; Adamo, C.; Clifford, S.; Ochterski, J.; Petersson, G. A.; Ayala, P. Y.; Cui, Q.; Morokuma, K.; Malick, D. K.; Rabuck, A. D.; Raghavachari, K.; Foresman, J. B.; Cioslowski, J.; Ortiz, J. V.; Stefanov, B. B.; Liu, G.; Liashenko, A.; Piskorz, P.; Komaromi, I.; Gomperts, R.; Martin, R. L.; Fox, D. J.; Keith, T.; Al-Laham, M. A.; Peng, C. Y.; Nanayakkara, A.; Gonzalez, C.; Challacombe, M.; Gill, P. M. W.; Johnson, B. G.; Chen, W.; Wong, M. W.; Andres, J. L.; Head-Gordon, M.; Replogle, E. S.; Pople, J. A. *Gaussian 98*, revision A9; Gaussian, Inc.: Pittsburgh, PA, 1998.
(39) Scott, A. P.; Radom, L. *J. Phys. Chem.* **1996**, *100*, 16502.
(40) Curtiss, L. A.; Raghavachari, K.; Redfern, P. C.; Rassolov, V.; Pople, J. A. *J. Chem. Phys.* **1998**, *109*, 7764.
(41) Baboul, A. G.; Curtiss, L. A.; Redfern, P. C.; Raghavachari, K. *J. Chem. Phys.* **1999**, *110*, 7650.
(42) Gordon, M. S.; Truong, T. N.; Bonderson, E. K. *J. Am. Chem. Soc.* **1986**, *108*, 1421.
(43) Moffat, H. K.; Jensen, K. F.; Carr, R. W. *J. Phys. Chem.* **1992**, *96*, 7683.
(44) Martin, J. G.; O'Neal, H. E.; Ring, M. A. *Int. J. Chem. Kinet.* **1990**, *22*, 613.
(45) Ring, M. A.; O'Neal, H. E. *J. Phys. Chem.* **1992**, *96*, 10848.
(46) Becerra, R.; Walsh, R. *J. Phys. Chem.* **1992**, *96*, 10856.
(47) Ho, P.; Coltrin, M. E.; Breiland, W. G. *J. Phys. Chem.* **1994**, *98*, 10138.
(48) Chambreau, S. D.; Zhang, J. S. *Chem. Phys. Lett.* **2001**, *343*, 482.
(49) Wang, L.; Zhang, J., manuscript in preparation.
(50) Curtiss, L. A.; Raghavachari, K.; Deutsch, P. W.; Pople, J. A. *J. Chem. Phys.* **1991**, *95*, 2433.
(51) Berkowitz, J.; Greene, J. P.; Cho, H.; Ruscic, B. *J. Chem. Phys.* **1987**, *86*, 1235.
(52) da Silva, A. J. R.; Pang, J. W.; Carter, E. A.; Neuhauser, D. *J. Phys. Chem. A* **1998**, *102*, 881.